Robust damping controller for synchronous generators under operational uncertainties

Sadegh Kamali [1], Masoud Hasani Marzooni [2] and Turaj Amraee [1]

[1] Faculty of Electrical Engineering, K.N. Toosi University of Technology, Tehran, Iran

[2] Energy and Electricity Economics Department, Niroo Research Institute, Tehran, Iran

Abstract- Power system stabilizers have been widely used to create sufficient damping against low-frequency oscillations in power systems. Due to appearing uncertainties in operational conditions of power systems, robust design of power system stabilizers is a crucial requirement for small signal stability. In this paper, a robust local damping controller is developed considering the possible uncertainties in operational conditions. The developed damping controller is optimized based on the H-infinity method in presence of uncertainties in electrical variables of the synchronous machine. In the proposed robust damping controller, only the practically available control signals such as the deviation of the rotor speed of the synchronous generators are used. To fulfill the robust and internal stabilities of the damping controller under a given horizon of operational uncertainties, a novel design based on the combination of the developed robust damping controller and the conventional power system stabilizer is introduced. Simultaneous damping of local oscillatory modes and the internal stability of the proposed robust controller is achieved via a multi-objective function. The efficacy of the proposed local damping controller is compared with the conventional power system stabilizer and a damping controller that is designed using the pole placement approach.

Keywords: Damping Controller, Genetic Algorithm, Optimization, Robust, Small Signal Stability, Synchronous Generator.

Emails (Sadegh Kamali: s.kamali@ee.kntu.ac.ir, Turaj Amraee (amraee@kntu.ac.ir), Masoud Hasani Marzooni: (mhasani@nri.ac.ir)

Nomenclature

$\Delta\delta$	Rotor angle of generator
H	Inertia constant of Generator
Δv_1	Output of terminal voltage transducer
Δv_2	Output signal of stabilizer's washout
Δv_s	Output signal of damping controller
$\Delta\phi_{fd}$	Magnetic flux of field circuit
ΔE_t	Terminal voltage of the generator
$\Delta\omega$	Rotor speed of generator
$\rho_{1,}\rho_2$	Weighting factors in the objective function
$K_1 to K_6$	Parameters of Heffron-Phillips Model
K_{cp}	Gain of conventional PSS
K_D	Damping torque coefficient
T_1, T_2	Time constants of conventional power system stabilizer
T_3	Time constant of excitation windings
T_m	Input mechanical torque
T_{r1}, T_{r2}	Time constants of robust controller
T_R	Time constant of voltage transducer
T_w	Time constant of Washout block
W_w	Weighting function of rotor speed uncertainty
W_δ	Weighting function of rotor-angle uncertainty
W_E	Weighting function of voltage uncertainty

1- Introduction

The stability of synchronous generators at all times is a prerequisite for the stable operation of power systems. Small signal rotor angle stability refers to the ability of a power system to maintain synchronism under small disturbances such as load perturbations. Small signal rotor angle instability problem is usually associated with insufficient damping of low-frequency oscillations. Traditionally power system stabilizers have been utilized to provide sufficient damping against local low-frequency oscillations at predetermined operating conditions [1]. Due to increasing the penetration level of renewable energy resources in nowadays power systems, as well as the rapid and unpredictable changes in operating conditions, the performance of the conventional damping controllers such as power system stabilizers is expected to be deteriorated. Therefore, the robust design of the damping controller has recently become the focus of literature on small signal stability of power systems. In [1, 2], a robust power system stabilizer has been developed for multi-machine power systems based on the optimization of stabilizer's parameters to reach a predefined value of damping based on the real parts of dominant eigenvalues of the linearized state-space matrix. In [3, 4], a power system stabilizer has been designed to achieve the maximum possible damping for low-frequency oscillations. Similar designs of power system stabilizers using different optimization algorithms have been proposed in [5]. The coordinated design of power system stabilizers and flexible AC transmission systems (FACTS) may be used to enhance the performance of conventional stabilizers [6-13]. The multi-band power system stabilizers have been addressed in literature as power oscillation damping tools. Multi-band power system stabilizers have their benefits and drawbacks and have not been used in practice due to the complexity in tuning. For example, each band of IEEE PSS4B has 18 setting parameters and this is a major challenge for such power system stabilizers. In [14, 15], the optimal tuning of multi-band power system stabilizers has been addressed for multi-machine power systems. Detailed tuning of the Multi-Band power system stabilizer (MB-PSS) is presented in [16].

To preserve the performance of controllers under volatile operating conditions, the robust design of damping controllers has been recently investigated in the literature. A robust PID controller based on the linear quadratic Gaussian approach for improving the frequency stability of power systems is proposed in [12]. In [17], a damping control method based on a robust self-triggered model predictive control is proposed using linearization of the power system model and determining the controller installation location through geometric measurements. In [18, 19], using the H-infinity method, a robust damping controller has been developed considering the load demand uncertainty. Some of the state variables utilized in [18] cannot be physically measured. In [20], based on the

Routh-Hurwitz criterion and Kharitonov theorem a robust power system stabilizer has been introduced for a single-machine infinite-bus (SMIB) system without considering uncertainties. Different techniques are mixed with robust technique to provide sufficient damping for small signal oscillation in power system such as periodic output feedback, pole placement method [21-23], variable structure method, quantitative feedback theory [24, 25] and sliding mode control [26-29]. Tuning of power system stabilizer using fuzzy logic has been investigated in [30-33]. In [34-36] the optimal control, adaptive control, and polynomial control are utilized for damping improvement and the parameters are tuned using optimization techniques.

There are different sources of uncertainty that can affect the damping control design. Uncertainties in system parameters, operational conditions, and time delay of the damping control are among the most important sources of uncertainties. In [37, 38], the uncertainties in the time delay of the damping control system especially in the measurement layer have been addressed. In [39], a robust damping controller is developed to suppress the low-frequency oscillations under load uncertainties. In [40], the uncertainty models based on both a set of operating conditions of the system and the lower and upper limits of the time delay are considered.
In multi-machine systems, inter-area and local oscillations affect the power system stability. The power system stabilizer is designed in a multi-machine power system using grey wolf optimization in [41]. The coordinated switching power system stabilizer is designed in[42] to enhance the stability of multi-machine power systems by switching between a bang-bang power system stabilizer and a conventional power system stabilizer based on fast and slow oscillations. Optimal placement and tuning of the power system stabilizer in multi-machine systems are presented in [43].

In literature, fewer efforts have been made to design a damping controller in the presence of operational uncertainties that appeared in the system state variables, such as speed and rotor angles, due to changes in the system's operational conditions. Also, in previously proposed approaches, the availability of utilized control signals of synchronous generators is not considered.

In this paper, a robust damping controller is developed based on the H-infinity method with considering operational uncertainties using the practical control signal. The main conurbation of this paper is as follows:

1- Unlike the previously proposed damping controllers, in this paper, the uncertainties in voltage magnitude at the generator terminal, uncertainty in rotor speed, and uncertainty in rotor angle are considered. All these three variables are changing based on the system conditions.
2- In the proposed robust damping controller, only the practically-available control signals (e.g.$\Delta\omega$) have been used. Additionally, to remove the risk of internal instability of the

proposed controller, a supplementary controller has been used.

3- Simultaneous damping of local oscillatory modes and the internal stability of the proposed robust controller is achieved via a multi-objective function.

The rest of this paper is organized as follows. In section 2, the linearized state-space model of the SMIB system is presented. The procedure of tuning conventional PSS is introduced in section 3. In section 4, the uncertainties of operational conditions are introduced. The details of the proposed robust damping controller are presented in section 5. The simulation results are discussed in section 6. Finally, the paper is concluded in section 7.

2- Mathematical modeling

2-1- Linear state-space model of SMIB system

The proposed damping controller can be designed for damping local or inter-area oscillation modes. The focus of this paper is to develop a local controller for damping local oscillatory modes. The design of a controller for damping inter-area oscillation modes (such as a wide-area damping controller using multi-band PSSs) can be addressed in separate research works. While the focus of the controller design is to damp local oscillatory modes, the single-machine infinite bus is sufficient. However, for damping inter-area oscillatory modes, a multi-machine power system should be considered. The state-space model of the SMIB is linearized as given in (1) -(5). The details of the nonlinear dynamic model of the SMIB system could be found in [44, 45].

$$\Delta\dot{\delta} = \omega\Delta\omega \tag{1}$$

$$\Delta\dot{\omega}(2Hs + K_D) = \Delta T_m - K_1\Delta\delta - K_1\Delta\phi_{fd} \tag{2}$$

$$\Delta\phi_{fd} + T_3\Delta\dot{\phi}_{fd} = -K_3(\Delta v_1 G_{ex}) - K_3K_4\Delta\delta \tag{3}$$

$$\Delta v_1 + T_R\Delta\dot{v}_1 = K_6\Delta\phi_{fd} + K_5\Delta\delta \tag{4}$$

$$\begin{pmatrix} \Delta\dot{\omega} \\ \Delta\dot{\delta} \\ \Delta\dot{\phi}_{fd} \\ \Delta\dot{v}_1 \end{pmatrix} = \begin{pmatrix} \frac{K_D}{2H} & -\frac{K_1}{2H} & -\frac{K_2}{2H} & 0 \\ \omega_0 & 0 & 0 & 0 \\ 0 & -\frac{1}{T_a} & -\frac{1}{T_a} & -\frac{K_a}{T_a} \\ 0 & \frac{K_5}{T_R} & \frac{K_6}{T_R} & -\frac{1}{T_R} \end{pmatrix} \times \begin{pmatrix} \Delta\omega \\ \Delta\delta \\ \Delta\phi_{fd} \\ \Delta v_1 \end{pmatrix} + \begin{pmatrix} \frac{1}{2H} \\ 0 \\ 0 \\ 0 \end{pmatrix} \times \Delta T_m \tag{5}$$

The linearized model of the dynamic system given in (1)-(5) is represented via the Heffron-Phillips model based on $K_1 to K_6$ coefficients as shown in Fig. 1. The $K_1 to K_6$ coefficients depend on

both the operating point and the design parameters of the synchronous machine [44]. Here the dynamic of governors (i.e. load frequency control) is ignored.

2-2- PSS Design

Conventional PSS (CPSS) are widely used to provide sufficient damping under small disturbances. PSS damps the low-frequency oscillations (LFO) by creating an additional component of damping torque in phase with the speed deviations. The CPSS must be designed to give the maximum damping under credible operating conditions. Different approaches have been proposed for tuning conventional PSS [18, 44]. Indeed the real part of all eigenvalues of the linearized state-space matrix must be negative and the lead-lag module must compensate for the phase lag between the exciter input and the electrical torque. The PSS contributes to the damping of oscillations over a range of frequencies.

As shown in Fig. 2, in this paper the conventional PSS is tuned using the speed deviation as the control signal. According to Fig. 2, the transfer function of the conventional PSS is expressed as follows:

$$G_{pss} = K_p\left(\frac{T_w s}{T_w s + 1}\right)\left(\frac{1 + T_1 s}{1 + T_2 s}\right) \tag{6}$$

where parameter K_p is the gain of PSS to suppress the low-frequency oscillations over a given range of frequencies (e.g. 0.1 Hz to 2 Hz). The linear dynamic model of the SMIB system in presence of PSS is expressed as follows:

$$\Delta\phi_{fd} = T_3\Delta\dot{\phi}_{fd} = K_3(-\Delta v_1 \times G_{ex}) + K_3(\Delta v_s \times G_{ex}) - K_3K_4\Delta\delta \tag{7}$$

$$\Delta\dot{v}_1 = \frac{K_5}{T_R}\Delta\omega + \frac{K_6}{T_R}\Delta\delta - \frac{1}{T_R}\Delta\phi_{fd} \tag{8}$$

$$\Delta\dot{v}_2 = \frac{K_{cp}K_D}{2H}\Delta\omega - \frac{K_{cp}K_1}{2H}\Delta\delta - \frac{K_{cp}K_2}{2H}\Delta\phi_{fd} - \frac{1}{T_w}\Delta v_2 + \frac{K_{cp}}{2H}\Delta T_m \tag{9}$$

$$\Delta\dot{v}_s = \frac{K_{cp}K_D}{2H}\frac{T_1}{T_2}\Delta\omega - \frac{K_{cp}K_1}{2H}\frac{T_1}{T_2}\Delta\delta - \frac{K_{cp}K_2}{2H}\frac{T_1}{T_2}\Delta\phi_{fd} - \frac{1}{T_2}\Delta v_2 + \left(-\frac{1}{T_w}\frac{T_1}{T_2} + \frac{1_1}{T_2}\right)\Delta v_s + \frac{K_{cp}}{2H}\frac{T_1}{T_2}\Delta T_m \tag{10}$$

Finally, the linear state-space model of the SMIB system including the PSS is introduced as follows:

$$\begin{pmatrix} \Delta\dot{\omega} \\ \Delta\dot{\delta} \\ \Delta\dot{\phi}_{fd} \\ \Delta\dot{v}_1 \\ \Delta\dot{v}_2 \\ \Delta\dot{v}_s \end{pmatrix} = \begin{pmatrix} \frac{K_D}{2H} & -\frac{K_1}{2H} & -\frac{K_2}{2H} & 0 & 0 & 0 \\ \omega_0 & 0 & 0 & 0 & 0 & 0 \\ 0 & -\frac{K_5 K_4}{T_s} & -\frac{1}{T_s} & -\frac{K_s G_{ex}}{T_s} & 0 & \frac{K_s G_{ex}}{T_s} \\ 0 & \frac{K_5}{T_R} & \frac{K_6}{T_R} & -\frac{1}{T_R} & 0 & 0 \\ \frac{-K_{cp} K_D}{2H} & \frac{-K_{cp} K_1}{2H} & \frac{K_{cp} K_2}{2H} & 0 & \frac{1}{T_w} & 0 \\ \frac{-K_{cp} K_D}{2H}\frac{T_1}{T_2} & -\frac{K_{cp} K_1}{2H}\frac{T_1}{T_2} & -\frac{K_{cp} K_2}{2H}\frac{T_1}{T_2} & 0 & -\frac{1}{T_2} & -\frac{1}{T_w}\frac{T_1}{T_2}+\frac{1_1}{T_2} \end{pmatrix} \times \begin{pmatrix} \Delta\omega \\ \Delta\delta \\ \Delta\phi_{fd} \\ \Delta v_1 \\ \Delta v_2 \\ \Delta v_s \end{pmatrix} + \begin{pmatrix} \frac{1}{2H} \\ 0 \\ 0 \\ 0 \\ \frac{K_{cp}}{2H} \\ \frac{K_{cp}}{2H}\frac{T_1}{T_2} \end{pmatrix} \Delta T_m \qquad (11)$$

2-3- Uncertainties in operational conditions

The parameters of the well-known linearized model of the SMIB system or Heffron–Phillips model depend highly on the system conditions. In other words, by changing the operating point of the system, the system model is changed too. These changes are well reflected in changes in rotor speed, rotor angle, and voltage magnitude. Therefore, to minimize the deterioration of damping control under varying operational conditions, the robust controller is utilized. Different structural or operational uncertainties may be considered in the robust design of a damping controller. Here the uncertainties in operational conditions including uncertainties in rotor speed, rotor angle, and terminal voltage are considered. Three different weighting functions including W_δ, W_ω and W_E are introduced for modeling uncertainties in rotor angle, speed, and terminal voltage respectively. The H-infinity norm of the weighting functions must be greater than the maximum possible uncertainty at different frequencies. To achieve a proper weighting function for rotor angle uncertainty, the frequency response of the transfer function of the linearized system (i.e. $H_\delta(s)$ as given in (12) according to Fig. 3) is depicted under different loading conditions. It is noted that the methods utilized to obtain the proper weighting function are different based on the nature of the controller design. In this problem, the change of system loading conditions causes a perturbation in the model as an ΔT_m. The frequency response of $H_\delta(s)$ must be evaluated for each random loading condition (Value of loading conditions is assumed to be $0.6\ to\ 1.5\ pu$). The obtained weighting function must be greater than the maximum frequency response (as shown in Fig. 1)

$$H_\delta(s) = \frac{\Delta\delta(s)}{p_1(s)} \qquad (12)$$

The weak and stiff systems represent extreme operating conditions. To achieve the maximum robustness against possible uncertainties, the frequency response of (12) for different values of perturbations (i.e. change of input mechanical torque $\Delta T_m(s)$) is shown in Fig. 3-a. The details of

assigning a proper weighting function based on the frequency response could be found in [46]. Based on the obtained frequency responses, the weighting function is selected as follows:

$$W_\delta(s) = 1.38\frac{s+1}{s+3} \tag{13}$$

where the constraint given in (14) is satisfied over a wide range of the frequency.

$$\| W_\delta^{-1} H_\delta(s) \| = \leq 1 \tag{14}$$

The weighting function for rotor angle can be designed by minimizing fitness function as given below:

Fitness function: $\| W_\delta^{-1} H_\delta(s) \| - 1$ (15)

Subject to

$$W_\delta = \frac{K(s+a)}{(s+b)} \tag{16}$$

$$\| W_\delta^{-1} H_\delta(s) \| = \leq 1 \tag{17}$$

Each W_δ that satisfies these constraints could be considered as a weighting function.

For rotor speed uncertainty, the frequency responses of the transfer function of the linearized system (i.e. $H_\omega(s)$ as given in (18)) is depicted under different loading conditions.

$$H_\omega(s) = \frac{\Delta\omega(s)}{p_2(s)} \tag{18}$$

Similar to the procedure for the weighting function of rotor angle, to achieve the maximum robustness against possible uncertainties the envelope of responses shown in Fig. 3-b, is selected as the weighting function of rotor speed as follows:

$$W_\delta = \frac{8}{(s+2)} \tag{19}$$

Finally for voltage uncertainty, the frequency responses of the transfer function of the linearized system (i.e. $H_E(s)$ as given in (20) is depicted under different loading conditions.

$$H_E(s) = \frac{\Delta E_t(s)}{p_3(s)} \tag{20}$$

In order to achieve the maximum robustness against possible uncertainties the envelope of responses shown in Fig. 3-c, is selected as the weighting function of terminal voltage as follows:

$$W_E = \frac{2.3}{(s+2)} \tag{21}$$

The weighting functions of uncertainties are now included in the linearized model of the SMIB system as shown in Fig. 4, where G_{en} represent the linear model of the system shown in Fig.1.

2-4- Design of the proposed robust damping controller

Two different designs are proposed for the robust damping controller of the SMIB system. The first damping controller, hereafter referred to as the first type controller considers the operational uncertainties without including the conventional PSS. It will be shown that the first type of robust controller suffers from internal instability while the robust stability is fulfilled. Also, internal stability is added as a constraint to the first-type controller to check the possibility of internal stability. However, the first-type controller even by adding the internal stability criterion fails to fulfill both the robust and internal stabilities simultaneously. The second-type controller combines the first-type controller with the conventional PSS to provide the robust damping of oscillations with satisfying the internal stability. The details of both damping controllers are presented below.

2-4-1- First type damping controller

Any proposed damping controller should satisfy both the robust and internal stabilities simultaneously. Internal stability refers to the stability of each input-output transfer function. Internal stability is a basic requirement for a practical feedback system. Internal stability guarantees that all signals in a system are bounded.

According to (22), to achieve a robust design of damping controller, the H-infinity norm of the transfer function (i.e. $\| N_{11} \|_\infty$) should be minimized [35]. The overall design of the first type controller has been illustrated in Fig. 5, where the Δ_δ, Δ_w and Δ_{Et} represent normalized uncertainty model (i.e. $(\| \Delta_\delta \|_\infty \le 1, \| \Delta_w \|_\infty \le 1 and \| \Delta_{Et} \|_\infty \le 1)$. According to Fig. 5, the transfer function of $[N_{11}]$ is defined as follows:

$$\begin{pmatrix} \Delta\omega \\ \Delta\delta \\ f \\ Z_1 \end{pmatrix} = [N] \times \begin{pmatrix} p_1 \\ p_2 \\ p_3 \\ \Delta T_m \end{pmatrix} = \begin{pmatrix} N_{11} & N_{12} \\ N_{21} & N_{22} \end{pmatrix} \times \begin{pmatrix} p_1 \\ p_2 \\ p_3 \\ \Delta T_m \end{pmatrix} \tag{22}$$

where the transfer function of $[N_{11}]$ may be determined according to (23). The robust stability criterion is defined as given in (24).

$$\begin{pmatrix} \Delta\omega \\ \Delta\delta \\ f \end{pmatrix} = [N_{11}] \times \begin{pmatrix} p_1 \\ p_2 \\ p_3 \end{pmatrix} \tag{23}$$

$$\| N_{11} \|_\infty < 1 \tag{24}$$

To design the first type of robust controller the optimization model given in (25)-(26) is minimized.

$$\min Z_{c1} = \| N_{11} \|_\infty \tag{25}$$

$$\max(real(poles(N))) \le 0.2 \tag{26}$$

2-4-2- Second type of damping controller

To fulfill the internal and robust stability criterion, the conventional PSS is added to the first type controller as shown in Fig. 6. The modified combinatorial damping controller, hereafter referred to as the second type controller is then optimized using a new multi-objective fitness function as follows:

$$\min . Z_{c2} = \rho_1 f_1 + \rho_2 f \tag{27}$$

$$f_1 = \max(real(poles(N))) \le 0.2 \tag{28}$$

$$f_2 = \| N_{11} \|_\infty < 1 \tag{29}$$

Subject to:

$$\| N_{11} \|_\infty < 1 \tag{30}$$

$$\max(real(poles(N))) \le 0.2 \tag{31}$$

where, f_1 maximizes the routine stability and f_2 maximizes internal stability. However, the critical value of each internal and retinue stability is considered as a constraint. The value of the damping factor must be tolerable in the excitation system. This is achieved using the constraint of (31), by which the minimum value of the real part of the poles is restricted $real(poles(N))$.According to the related constraints, any set of weighting factors preserves stability (i.e.) $\| N_{11} \|_\infty < 1$ and the real part of dominant oscillatory mode is less than -0.2 (i.e. $(real(poles(N))) \le 0.2$).

The multi-objective function given in (27) tries to satisfy the internal and robust stabilities via the proper selection of weighting factors ρ_1 and ρ_2 .

2-5- Extending the proposed method to a Multi-Machine system

Fig.7 shows the configuration of the ith-machine of a multi-machine power system, where N synchronous generators are connected by transmission lines. The entire N-machine power system is equipped with PSSs and the proposed robust controller. Details of this multi-machine dynamic model could be found in[47]. All procedures of designing the robust controller could be followed as demonstrated in Sections 4 and 5.

3- Simulation Results in SMIB system

In this section, the performance of both proposed damping controllers is investigated over the SMIB system. The dynamic data of the SMIB system has been given in Appendix A. In part A, the simulation results of the first type controllers, and in part B the results of the second type damping controller are presented. Also, to verify the performance of the proposed controllers, time simulations under the step changes of inputs are presented in Part C. The proposed robust damping controllers are optimized using Genetic Algorithm.

3-1- Part A.

The first type of damping controller is optimized to obtain the minimum value of $\| N_{11} \|_\infty$. The optimal parameters of the first type controller are obtained as $T_{r1} = 0.1854, T_{r2} = 5.125$ and $K_{RC} = 42.651$. The eigenvalues of the linearized SMIB model (i.e. the linearized system shown in Fig. 7) have been reported in Table I. It can be seen that there is an unstable oscillatory mode as $0.06913 \pm j6.3672$.

According to Fig. 8, the best amount of $\| N_{11} \|_\infty$ is equal to 0.72 using the genetic algorithm. The parameters of the genetic algorithm are set as follows: The initial population is 200, the cross-over is a scattered function, the mutation is assumed using a Uniform function with a Rate of 0.009, and the maximum iteration is assumed as 200. The singular value of the proposed robust controller has been illustrated in Fig. 9. Unlike the acceptable value of $\| N_{11} \|_\infty$, it is evident that the first type of robust controller results in internal instability of the SMIB system. Therefore, the internal stability is added to the optimization problem of the first type controller as a constraint and the modified controller is re-optimized. The variations of the cost function of the modified first type controller have been illustrated in Fig. 10. It can be seen that the best value of the proposed robust damping controller is equal to $\| N_{11} \|_\infty$ =3.38 which violates the robust stability of the system. It is concluded that the proposed first type damping controller even with the described modification is not able to fulfill both internal and robust stability simultaneously. To this end, the second type of damping controller is implemented as given in the next part.

3-2- Part B.

In this part, the proposed second type damping controller is optimized using the Genetic Algorithm. The optimal parameters of the second type controller are obtained as given in Table II. According to [44], the real part of dominant oscillating modes must be smaller than -0.20. The inverse of the real part of the dominant modes (i.e. closed-loop poles or the eigenvalues of the linearized system state matrix are close to the imaginary axis in the mode plane) refers to the time constant of the exponential trajectories of state variables. Therefore, a real part of -0.20 refers to a time constant of 5 seconds. If we assume that the variations of the state variables decay exponentially, then after 4 to 5-time constants, these variations die out. In other words, under a real value of -0.20, the low-frequency oscillations should die out within 20 seconds to 25 seconds.

Also the value of the H-infinity function (i.e. $\| N_{11} \|_\infty$ must be lower than 1. It is noted that the proposed controller is stable over the defined range of operating conditions provided that the constraint of $\| N_{11} \|_\infty < 1$ is fulfilled. Therefore, the weighting factors in the utilized multi-objective function (i.e. the objective function given in (27)) have been considered as $(\rho_1, \rho_2) = (5,1)$. The variations of the cost function of the second type controller have been illustrated in Fig. 11. It can be seen that the best value of the proposed robust damping controller is obtained as $Z_{c1} = -0.29077$ and the maximum real part of poles is equal to -0.22.

The eigenvalues of the linearized SMIB model using the second type damping controller have been reported in Table III. It can be seen that there is no unstable oscillatory mode. The singular value of the proposed robust controller has been illustrated in Fig. 12. It can be seen that the second type of robust controller fulfills both internal and robust stability simultaneously.

According to the optimal parameters obtained by the genetic algorithm, the transfer functions of the robust controller and the transfer function of conventional PSS are given in (32) and (33) respectively.

$$T_{PSS} = 9.454 \frac{0.5476s + 1}{0.1s + 1} \times \frac{5s}{5s + 1} \tag{32}$$

$$T_{robust} = 58.86 \frac{0.13406s + 1}{4.1263s + 1} \tag{33}$$

3-3- Part C. Time simulation

In this section, the performance of the proposed robust damping controllers under step changes of some inputs is investigated using time simulations for rotor angle, rotor speed, and electrical power. The time variations of rotor speed under different step-change in ΔT_m and ΔV_{ref} are shown in

Fig. 13. Furthermore, to the analysis of the system for change in operation condition the equivalent reactance between the machine terminal and the infinite bus is changed from 0.4 to 2.5 Pu. The system responses for this equivalent reactance have been shown in Fig. 14, it can be seen that the performance of the second type damping controller is better than the first type damping controller.

To give a comparative analysis, dominant eigenvalues are evaluated for three different types of damping controller by changing the operational conditions. As shown in Fig. 15, in case of using the pole placement controller, the dominant eigenvalues move to the unstable area. However, using the proposed robust controller, the stability of system is fulfilled under changing the operational conditions. In Fig. 15, the variations of two dominant modes (i.e. two different dominant eigenvalues) are illustrated for each damping controller. Other eigenvalues are far from the imaginary axis.

4- Simulation Results in Multi Machine System

In this section, the performance of the proposed damping controller is investigated over the Multi-machine power system. The proposed method is implemented in IEEE 39-bus test system. All data of this test system can be found in [48].

4-1- Implementation of the conventional controller in IEEE 39-Bus Test System

As mentioned in section 5.2, the robust stability criterion is ($\| N_{11} \|_\infty < 1$) and the internal stability constraint is (i.e. $\max(real(poles(N))) < -0.2$ All parameters of the Conventional PSS of the system are reported in Table IV. The values of critical eigenvalues in normal loading is given in Table V. The singular values of the test system are shown in Fig. 16. According to Fig. 16, the infinite norm of the system is 1.90. Therefore, the system is internally unstable.

4-2- Implementation of the proposed second type robust controller in IEEE 39-Bus test system

In order to design the robust controller, we first optimize the value of the objective function for $\rho_1 = 0$ (i.e. only infinite norm of N_{11} is considered). In this case, the value of the objective function is 0.654. In the second step, we optimize the objective function considering $\rho_2 = 0$ (i.e. only real part of eigenvalues is considered). In this case, the value of the objective function is -0.61. Therefore the values of ρ_2 and ρ_1 are assumed to be as 1.07 and 1 respectively. The mean and best values of the objective function using GA algorithm is shown in Fig. 17. The best value is 0.43229 in which, f_1=-0.5287 and f_2=0.998. All parameters of the proposed controller are given in Table VI. As shown in Fig. 18 the singular values of the system are lower than 1.

4-3- Comparison of the controllers

In this section to verify the performance of the proposed controller, the operating point including generation and loading pattern are changed up to 20% randomly. The step response of the system with conventional PSS controller and the second type robust controller are shown in Fig. 19 and Fig. 20 respectively. As shown in Fig. 19 and Fig. 20, the step response of the system is not stable. However, the step response of the system with the second type robust controller is stable.

5- Conclusions

In this paper, the operational uncertainties including the uncertainties in rotor speed, rotor angle, and terminal voltage were included in the robust design of the damping controller. Two different designs for low-frequency oscillation damping controllers were developed. The major findings of this paper are summarized as follows. 1) Without considering the conventional PSS the proposed damping controller (i.e. the first type design) results in internal instability. However, the second type of damping controller in combination with the conventional PSS fulfills both internal and robust stability simultaneously. 2) By doing a comparative analysis, it was shown that the CPSS and Pole Placement Damping controllers both result in small-signal instability, and the dominant eigenvalues of the state space matrix enter the unstable area (i.e. the area where the real parts of the eigenvalues are positive). However, the proposed damping controller in this paper locates the eigenvalues far from the imaginary axis and the real parts of the dominant oscillatory modes are all lower than -1, which implies the strong small-signal stability of the system under operational uncertainties. Since the time constant of exponential variations of the state variables is equal to the inverse of the real part of dominant modes or eigenvalues, a real part of -1 says that the time constant of exponential time variations (i.e. exponential decay) of state variables is equal to 1 second. Therefore, the oscillations die out within 4 to 5 seconds. Indeed, we can assume that the oscillations die out after 4 to 5 time-constant. 3) In order to validate the modal analysis, the performance of the developed damping controllers was verified using both modal analysis and time simulations. The presented time-domain simulations confirmed the effectiveness of the proposed controller. The coordination of the proposed second type controller in a multi-machine power system to damp both local and inter-area oscillation modes is an open question for further researches.

REFERENCES

[1] Liu, J., Yang, Z., Zhao, J., et al. "Explicit Data-Driven Small-Signal Stability Constrained Optimal Power Flow", *IEEE Transactions on Power Systems*, (2021).

[2] Bento, M. E., "A hybrid particle swarm optimization algorithm for the wide-area damping control design", *IEEE Transactions on Industrial Informatics*, **18**(1), pp. 592-599 (2021).

[3] Abedinia, O., Amjady, N., Izadfar, H., et al. "Multi-machine power system oscillation damping: Placement and tuning PSS VIA multi-objective HBMO", *International Journal of Technical and Physical Problems of Engineering*, **4**(3), pp. 12-20 (2012).

[4] Saadatmand, M., Mozafari, B., Gharehpetian, G.B., et al. "Optimal coordinated tuning of power system stabilizers and wide‐area measurement‐based fractional‐order PID controller of large‐scale PV farms for LFO damping in smart grids", *International Transactions on Electrical Energy Systems*, **31**(2), pp. 1-19 (2021).

[5] Dubey, M. and Gupta, P. "Design of Genetic-Algorithm based robust power system stabilizer", *International Journal of Computational Intelligence*, **2**(1), pp. 48-52 (2005).

[6] Hasanvand, H., Arvan, M.R., Mozafari, B., et al. "Coordinated design of PSS and TCSC to mitigate interarea oscillations", *International Journal of Electrical Power & Energy Systems*, **78**, pp. 194-206 (2016).

[7] Fallahi, H., Aghamohammadi, M., Parizad, A., et al. "Enhancing power system oscillation damping using coordination between PSS and SVC", *2009 International Conference on Electric Power and Energy Conversion Systems,(EPECS)*, IEEE, pp. 1-7 (2009).

[8] Ramirez‐Gonzalez, M., Castellanos‐Bustamante, R., Calderon‐Guizar, J.G., et al. "Coordinated design of fuzzy supplementary controllers for generator and STATCOM voltage regulators using bat algorithm optimization", *International Transactions on Electrical Energy Systems*, **26**(9), pp. 1847-1862 (2016).

[9] Shahgholian G. and Faiz, J. "Coordinated control of power system stabilizer and FACTS devices for dynamic performance enhancement—State of art", *2nd International Conference on Intelligent Energy and Power Systems (IEPS)*, IEEE, pp. 1-6 (2016).

[10] Devarapalli, R., Bhattacharyya, B., Kumar, V., et al. "Improved moth flame optimization in systematization of STATCOM and PSS", *Advances in Smart Grid Automation and Industry 4.0*: Springer, pp. 481-491 (2021).

[11] Guesmi, T., Alshammari, B.M., Almalaq, Y., et al. "New coordinated tuning of SVC and PSSs in multimachine power system using coyote optimization algorithm", *Sustainability*, **13**(6), pp. 1-18 (2021).

[12] Khamies, M., Magdy, G., Ebeed, M., et al. "A robust PID controller based on linear quadratic gaussian approach for improving frequency stability of power systems considering renewables", *ISA transactions*, **117**, pp. 118-138, (2021).

[13] Li, X., Peng, K., Zhang, X., et al. "Robust stability control for high frequency oscillations in flexible DC distribution systems", *International Journal of Electrical Power & Energy Systems*, **137**, (2022).

[14] Khodabakhshian, A., Hemmati, R. and Moazzami, M. "Multi-band power system stabilizer design by using CPCE algorithm for multi-machine power system", *Electric Power Systems Research*, **101**, pp. 36-48 (2013).

[15] Sabo, A., Abdul Wahab, N.I., Lutfi Othman, M., et al. "Artificial Intelligence-Based Power System Stabilizers for Frequency Stability Enhancement in Multi-machine Power Systems", *IEEE Access*, **9**, pp. 166095-166116 (2021).

[16] Kamwa, I., Grondin, R. and Trudel, G. "IEEE PSS2B versus PSS4B: the limits of performance of modern power system stabilizers", *IEEE transactions on power systems*, **20**(2), pp. 903-915 (2005).

[17] Nie, Y., Liu, T., Wang, Z. and Zhao, Y. "Wide-area damping power system control based on robust self-triggered model predictive control", *International Journal of Electrical Power & Energy Systems*, **141**, (2022).

[18] Soliman, M. "Robust non-fragile power system stabilizer", *International Journal of Electrical Power & Energy Systems*, **64**, pp. 626-634 (2015).

[19] Rokrok, E., Dehghaninejad, S. and Poursaeed, A.H. "Adaptive Delay Compensator Based H_2/H_∞ Wide-Area Controller to Improve the Damping of Inter-Area Oscillations", *International Journal of Industrial Electronics Control and Optimization*, **5**(2), pp. 189-204 (2022).

[20] Soliman, M., Emara, H., Elshafei, A., et al. "Robust output feedback power system stabilizer design: an LMI approach", *2008 IEEE Power and Energy Society General Meeting-Conversion and Delivery of Electrical Energy in the 21st Century*, IEEE, pp. 1-8 (2008).

[21] Abido, M. "Pole placement technique for PSS and TCSC-based stabilizer design using simulated annealing", *International journal of electrical power & energy systems*, **22**(8), pp. 543-554 (2000).

[22] Furini, M., Pereira, A. and Araujo, P. "Pole placement by coordinated tuning of Power System Stabilizers and FACTS-POD stabilizers", *International Journal of Electrical Power & Energy Systems*, **33**(3), pp. 615-622 (2011).

[23] Kashki, M., Abido, M. and Abdel-Magid, Y. "Pole placement approach for robust optimum design of PSS and TCSC-based stabilizers using reinforcement learning automata", *Electrical Engineering*, **91**(7), pp. 383-394 (2010).

[24] Singh, N., Pratap, B. and Swarup, A. "Robust control design of variable speed wind turbine using quantitative feedback theory", *Proceedings of the Institution of Mechanical Engineers, Part A: Journal of Power and Energy*, **232**(6), pp. 691-705 (2018).

[25] Hemmati, R. "Power system stabilizer design based on optimal model reference adaptive system", *Ain Shams Engineering Journal*, **9**(2), pp. 311-318 (2018).

[26] Saoudi, K. and Harmas, M. "Enhanced design of an indirect adaptive fuzzy sliding mode power system stabilizer for multi-machine power systems", *International Journal of Electrical Power & Energy Systems*, **54**, pp. 425-431 (2014).

[27] Nechadi, E., Harmas, M., Hamzaoui, A., et al. "A new robust adaptive fuzzy sliding mode power system stabilizer", *International Journal of Electrical Power & Energy Systems*, **42**(1), pp. 1-7 (2012).

[28] Bandal, V., Bandyopadhyay, B. and Kulkarni, A. "Output feedback fuzzy sliding mode control technique based power system stabilizer (PSS) for single machine infinite bus (SMIB) system", *2005 IEEE International Conference on Industrial Technology*, pp. 341-346 (2005).

[29] Ray, P.K., Paital, S.R., Mohanty, A., et al. "A robust power system stabilizer for enhancement of stability in power system using adaptive fuzzy sliding mode control", *Applied Soft Computing*, **73**, pp. 471-481 (2018).

[30] Ramirez-Gonzalez M. and Malik, O. "Self-tuned power system stabilizer based on a simple fuzzy logic controller", *Electric Power Components and Systems*, **38**(4), pp. 407-423 (2010).

[31] Pahasa, J. and Ngamroo, I. "Adaptive power system stabilizer design using optimal support vector machines based on harmony search algorithm", *Electric Power Components and Systems*, **42**(5), pp. 439-452 (2014).

[32] You, R., Nehrir, M. and Pierre, D. "Controller design for SVC and TCSC to enhance damping of power system oscillations", *Electric Power Components and Systems*, **35**(8), pp. 871-884 (2007).

[33] Ebrahimian, H., Gollou, A.R., Bayramzadeh, F., et al. "Multimachine power system stabilizer based on optimal multistage fuzzy PID attendant honey bee mating optimization", *Complexity*, **21**(6), pp. 234-245 (2016).

[34] Sundareswaran K. and Razia Begum, S. "Genetic tuning of a power system stabilizer", *European transactions on electrical power*, **14**(3), pp. 151-160 (2004).

[35] Shokouhandeh H. and Jazaeri, M. "An enhanced and auto‐tuned power system stabilizer based on optimized interval type‐2 fuzzy PID scheme", *International Transactions on Electrical Energy Systems*, **28**(1), Doi: 10.1002/etep.2469 (2018).

[36] Karnik, S., Raju, A. and Raviprakasha, M. "Robust tuning of power system stabilizer using a non-iterative Taguchi design technique", *Electric Power Components and Systems*, **37**(3), pp. 239-252 (2009).

[37] Mou, Q., Ye, H. and Liu, Y. "Nonsmooth optimization-based WADC tuning in large delayed cyber-physical power system by interarea mode tracking and gradient sampling", *IEEE Transactions on Power Systems*, **34**(1), pp. 668-679 (2018).

[38] Li, Y., Zhou, Y., Liu, F., et al. "Design and implementation of delay-dependent wide-area damping control for stability enhancement of power systems", *IEEE Transactions on Smart Grid*, **8**(4), pp. 1831-1842 (2016).

[39] Maherani, M., Erlich, I. and Krost, G. "Fixed order non-smooth robust H∞ wide area damping controller considering load uncertainties", *International Journal of Electrical Power & Energy Systems*, **115**, Doi: 10.1016/j.ijepes.2019.105423 (2020).

[40] Bento, M.E. "Fixed low-order wide-area damping controller considering time delays and power system operation uncertainties", *IEEE Transactions on Power Systems*, **35**(5), pp. 3918-3926 (2020).

[41] Devarapalli, R., Bhattacharyya, B., Sinha, N.K., et al. "Amended GWO approach based multi-machine power system stability enhancement", *ISA transactions*, **109**, pp. 152-174 (2021).

[42] Liu, Y., Wu, Q., Kang, H., et al. "Switching power system stabilizer and its coordination for enhancement of multi-machine power system stability", *CSEE Journal of Power and Energy Systems*, **2**(2), pp. 98-106 (2016).

[43] Keumarsi, V., Simab, M. and Shahgholian, G. "An integrated approach for optimal placement and tuning of power system stabilizer in multi-machine systems", *International Journal of Electrical Power & Energy Systems*, **63**, pp. 132-139 (2014).

[44] Machowski, J., Bialek, J. and Bumby, J. *Power System Dynamics: Stability and Control*. John Wiley & Sons (2011).

[45] Dysko, A., Leithead, W.E. and O'Reilly, J. "Enhanced power system stability by coordinated PSS design", *IEEE Transactions on Power Systems*, **25**(1), pp. 413-422 (2010).

[46] Zhou, K. and Doyle, J.C. *Essentials of Robust Control*, Prentice hall Upper Saddle River, NJ (1998).

[47] Wang, H. and Du, W. *Analysis and Damping Control of Power System Low-frequency Oscillations*, Springer (2016).

[48] Pai, M.A. "APPENDIX A: 10 Machine system data" In *Energy Function Analysis for Power System Stability*, Springer (1989)

Figures Captions

Tables Captions

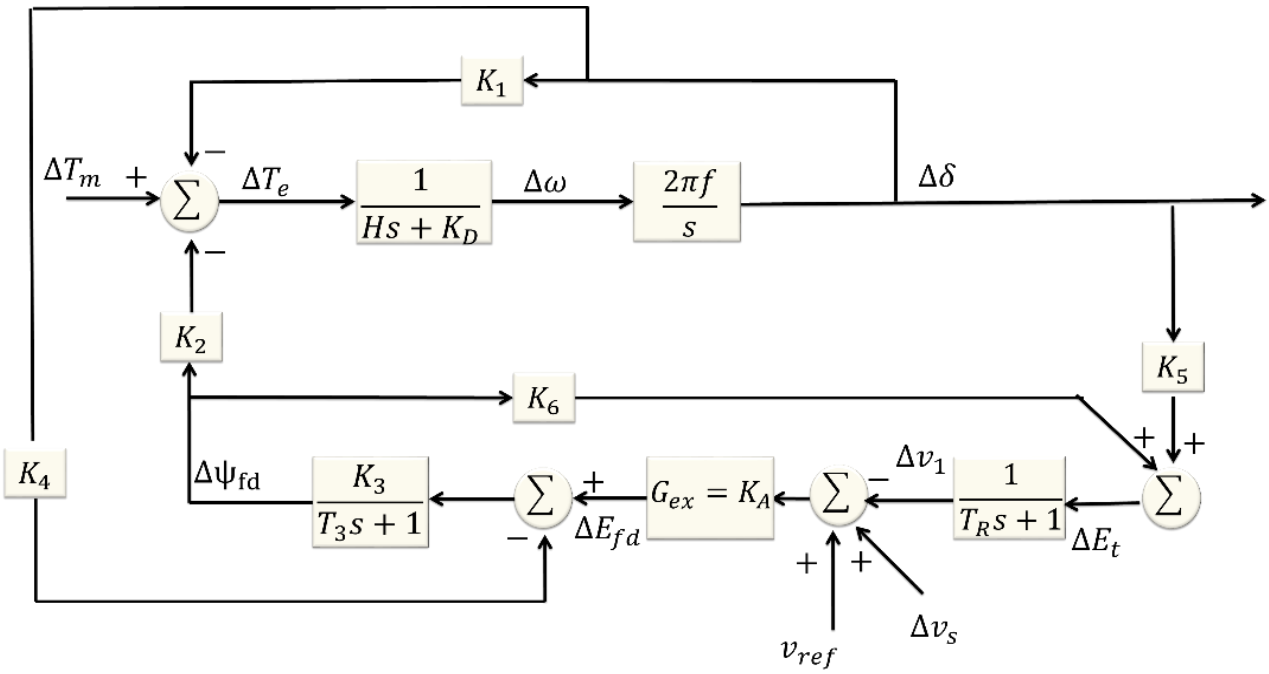
K_1
ΔT_m
ΔT_e
$\frac{1}{Hs + K_D}$
$\Delta\omega$
$\frac{2\pi f}{s}$
$\Delta\delta$
K_2
K_5
K_6
K_4
$\Delta\psi_{fd}$
$\frac{K_3}{T_3 s + 1}$
ΔE_{fd}
$G_{ex} = K_A$
Δv_1
$\frac{1}{T_R s + 1}$
ΔE_t
v_{ref}
Δv_s

Fig. 1

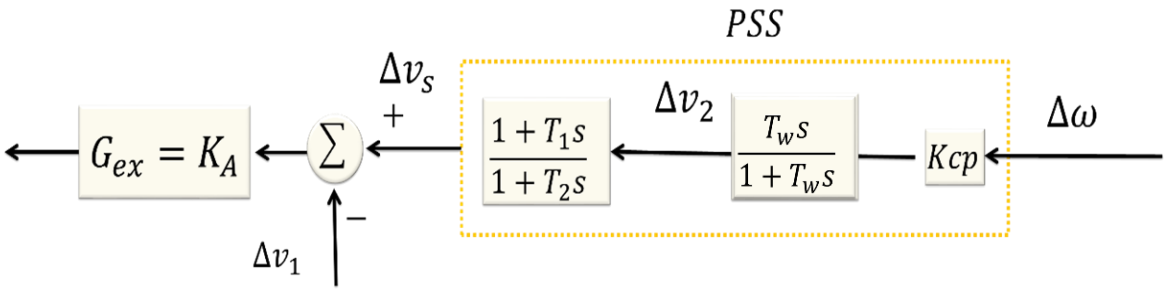
PSS
Δv_s
+
Δv_2
$\Delta\omega$
$G_{ex} = K_A$
$\sum$
$\frac{1+T_1 s}{1+T_2 s}$
$\frac{T_w s}{1+T_w s}$
Kcp
−
Δv_1

Fig. 2

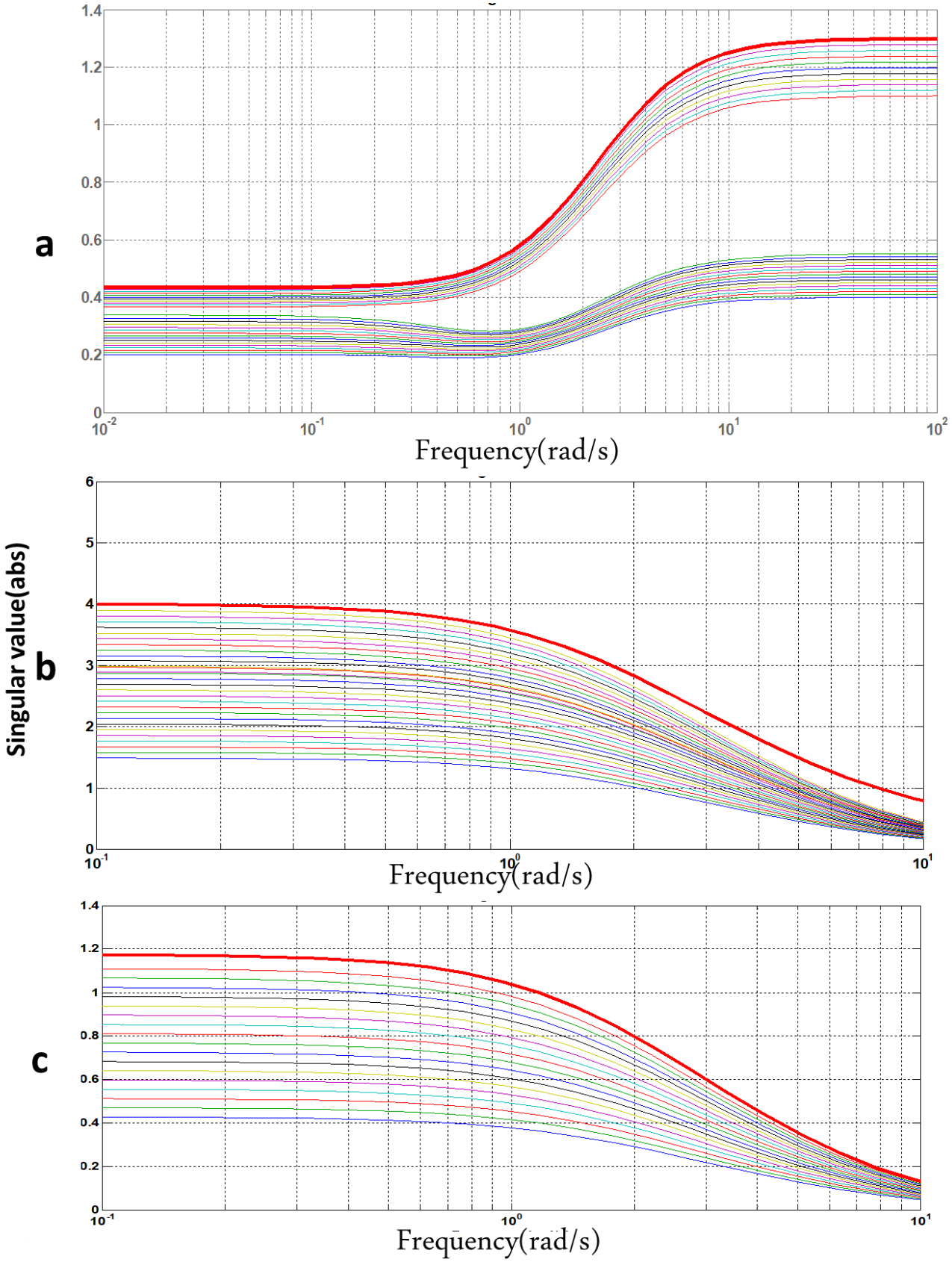
a
Frequency(rad/s)
Singular value(abs)
b
Frequency(rad/s)
c
Frequency(rad/s)

Fig. 3

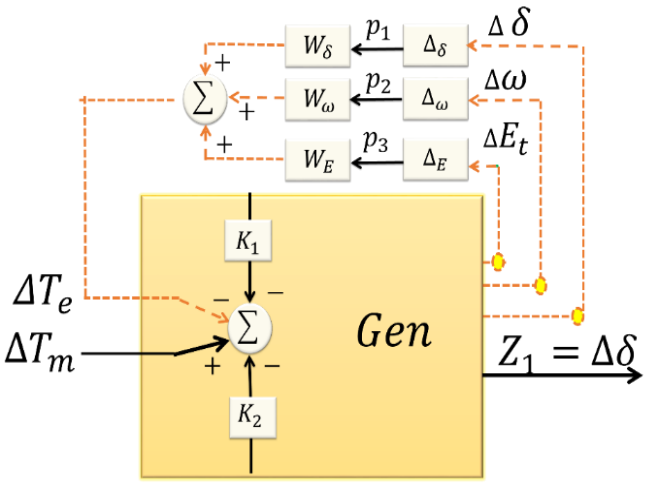
W_δ
p_1
Δ_δ
$\Delta\delta$
W_ω
p_2
Δ_ω
$\Delta\omega$
W_E
p_3
Δ_E
ΔE_t
K_1
K_2
ΔT_e
ΔT_m
Gen
$Z_1 = \Delta\delta$

Fig. 4

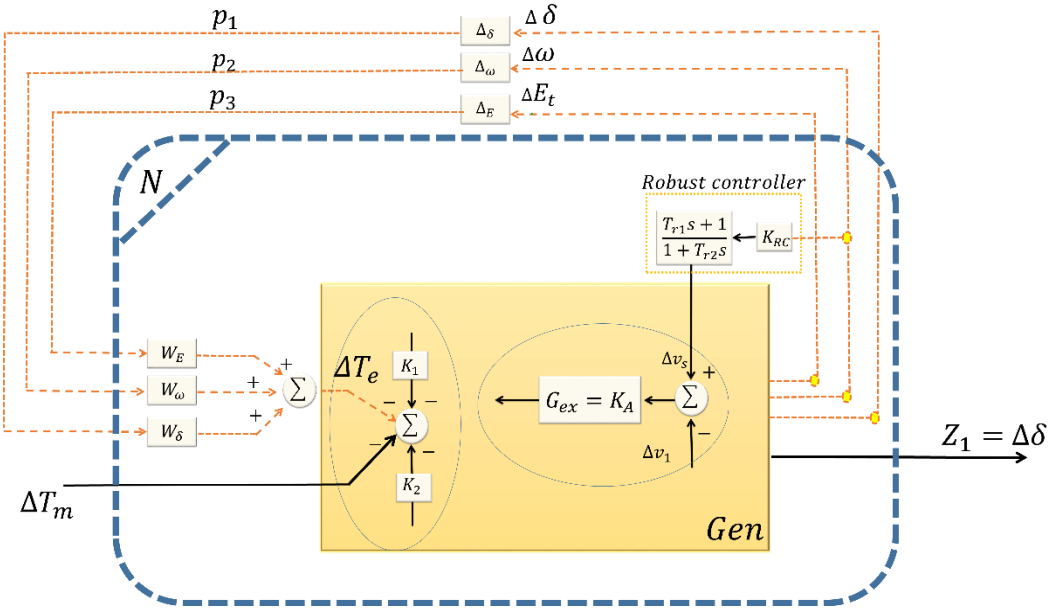
p_1
p_2
p_3
Δ_δ
Δ_ω
Δ_E
$\Delta\,\delta$
$\Delta\omega$
ΔE_t
N
Robust controller
$\frac{T_{r1}s+1}{1+T_{r2}s}$
K_{RC}
W_E
W_ω
W_δ
ΔT_e
K_1
K_2
$G_{ex} = K_A$
Δv_s
Δv_1
Gen
ΔT_m
$Z_1 = \Delta\delta$

Fig. 5

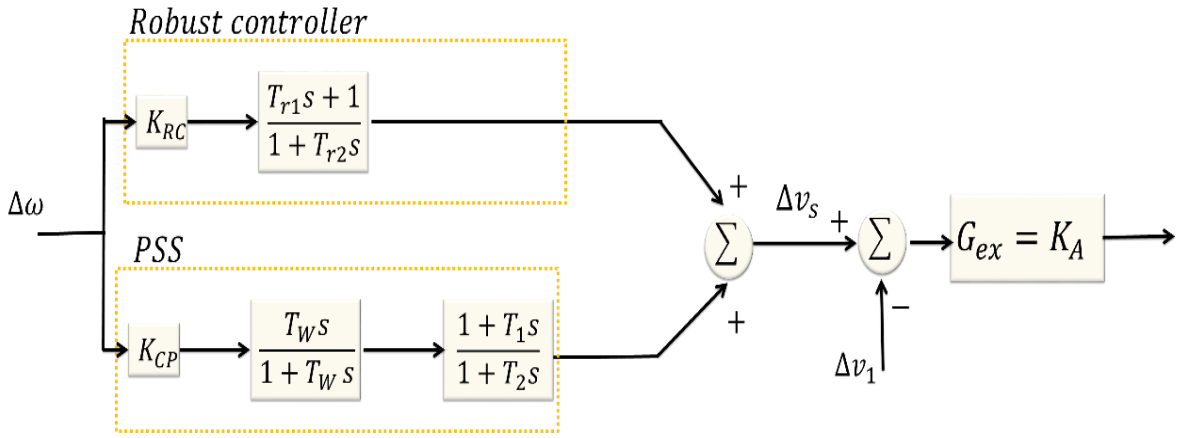
Robust controller
K_{RC}
$\frac{T_{r1}s+1}{1+T_{r2}s}$
$\Delta\omega$
PSS
K_{CP}
$\frac{T_W s}{1+T_W s}$
$\frac{1+T_1 s}{1+T_2 s}$
+
+
Δv_s
+
−
Δv_1
$G_{ex} = K_A$

Fig. 6

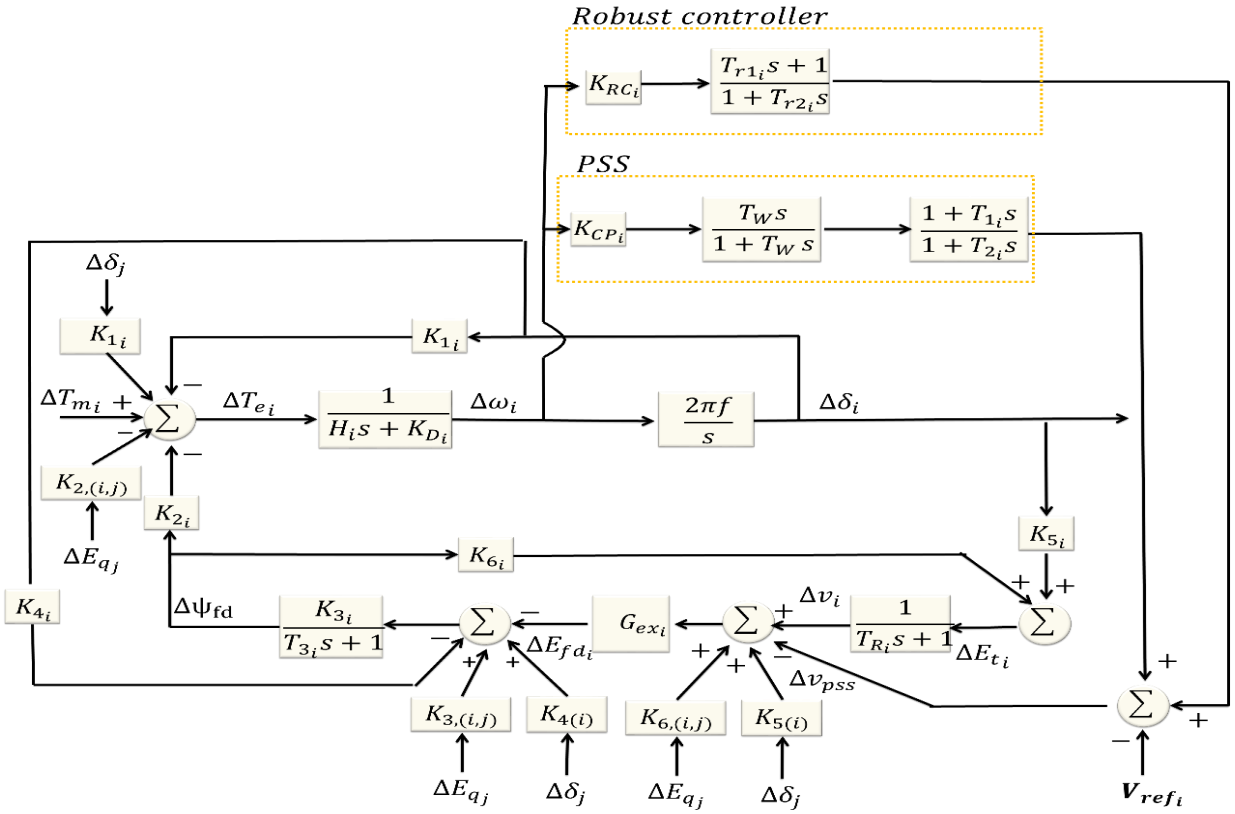
Robust controller
K_{RC_i}
$\frac{T_{r1_i}s+1}{1+T_{r2_i}s}$
PSS
K_{CP_i}
$\frac{T_W s}{1+T_W s}$
$\frac{1+T_{1_i}s}{1+T_{2_i}s}$
$\Delta\delta_j$
K_{1_i}
K_{1_i}
ΔT_{m_i}
ΔT_{e_i}
$\frac{1}{H_i s+K_{D_i}}$
$\Delta\omega_i$
$\frac{2\pi f}{s}$
$\Delta\delta_i$
$K_{2,(i,j)}$
K_{2_i}
ΔE_{q_j}
K_{5_i}
K_{6_i}
K_{4_i}
$\Delta\psi_{fd}$
$\frac{K_{3_i}}{T_{3_i}s+1}$
G_{ex_i}
Δv_i
$\frac{1}{T_{R_i}s+1}$
ΔE_{t_i}
ΔE_{fd_i}
Δv_{pss}
$K_{3,(i,j)}$
$K_{4(i)}$
$K_{6,(i,j)}$
$K_{5(i)}$
ΔE_{q_j}
$\Delta\delta_j$
ΔE_{q_j}
$\Delta\delta_j$
V_{ref_i}

Fig. 7

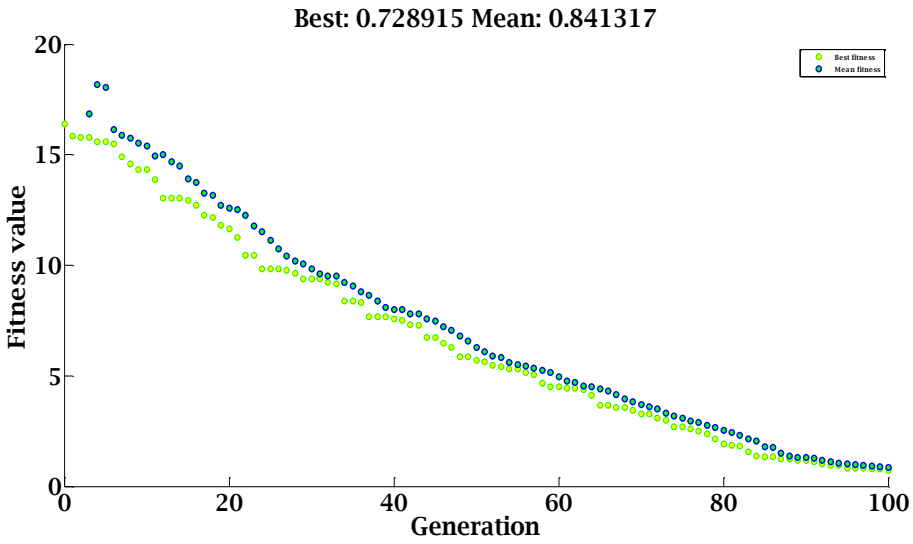
Best: 0.728915 Mean: 0.841317
Best fitness
Mean fitness
Fitness value
Generation
0
5
10
15
20
0
20
40
60
80
100

Fig. 8

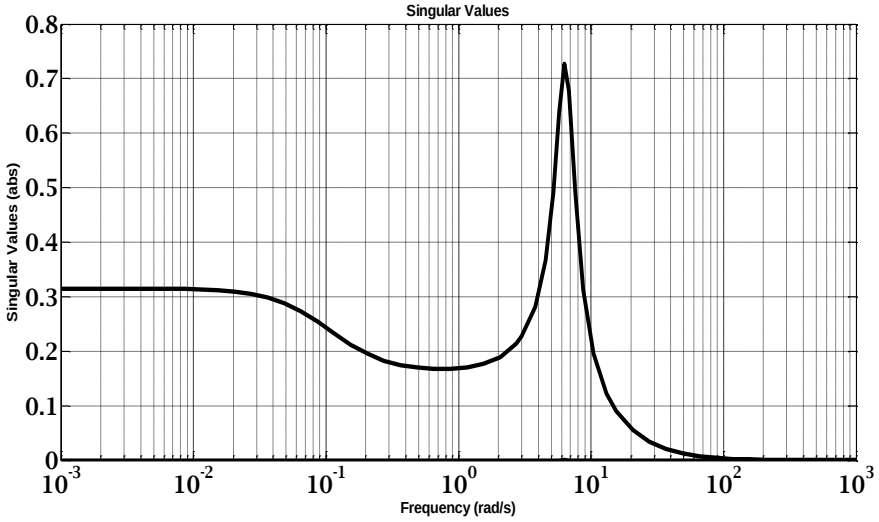
Singular Values
Singular Values (abs)
0.8
0.7
0.6
0.5
0.4
0.3
0.2
0.1
0
10^-3
10^-2
10^-1
10^0
10^1
10^2
10^3
Frequency (rad/s)

Fig. 9

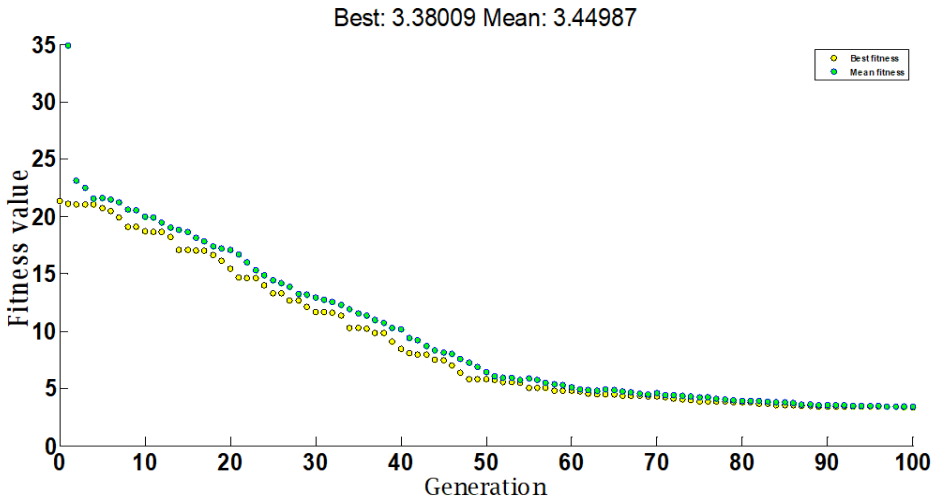
Best: 3.38009 Mean: 3.44987
Best fitness
Mean fitness
Fitness value
Generation
0
5
10
15
20
25
30
35
0
10
20
30
40
50
60
70
80
90
100

Fig. 10

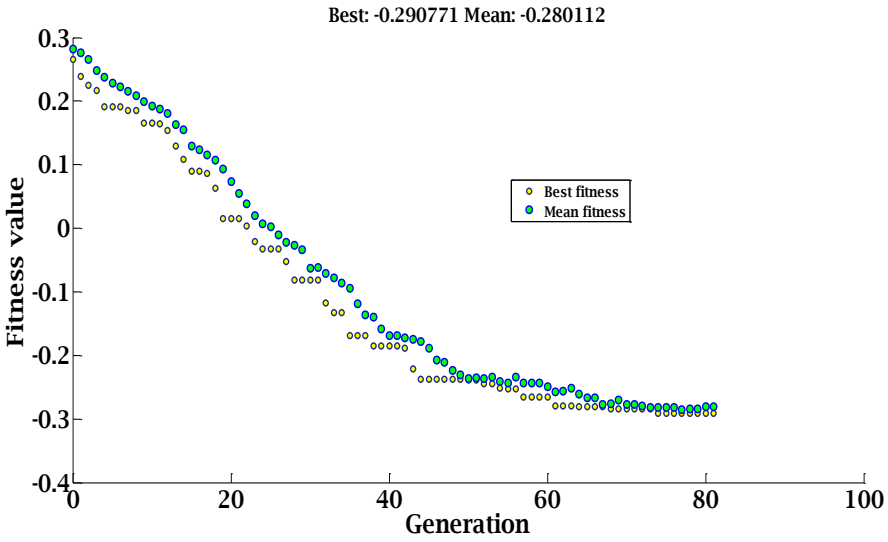
Best: -0.290771 Mean: -0.280112
Best fitness
Mean fitness
Fitness value
Generation
0.3
0.2
0.1
0
-0.1
-0.2
-0.3
-0.4
0
20
40
60
80
100

Fig. 11

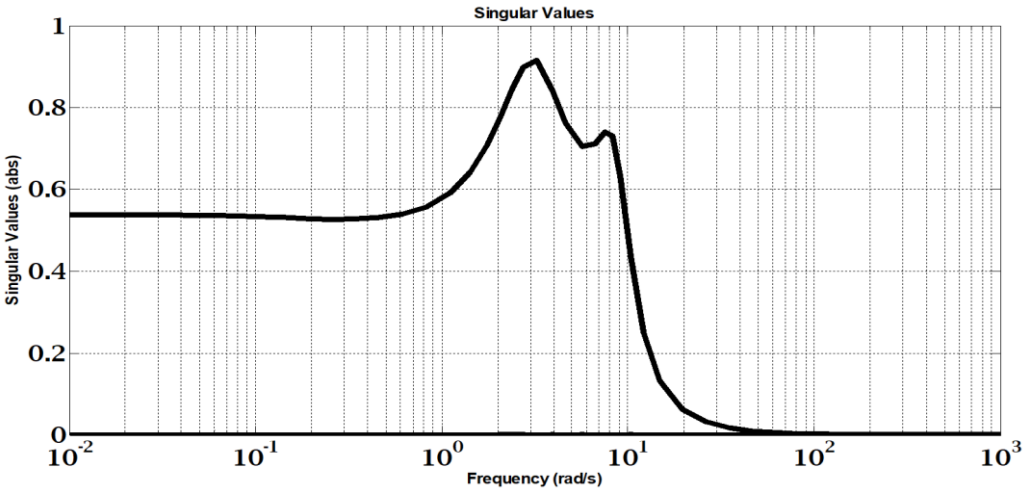
Singular Values
Singular Values (abs)
1
0.8
0.6
0.4
0.2
0
10^-2
10^-1
10^0
10^1
10^2
10^3
Frequency (rad/s)

Fig. 12

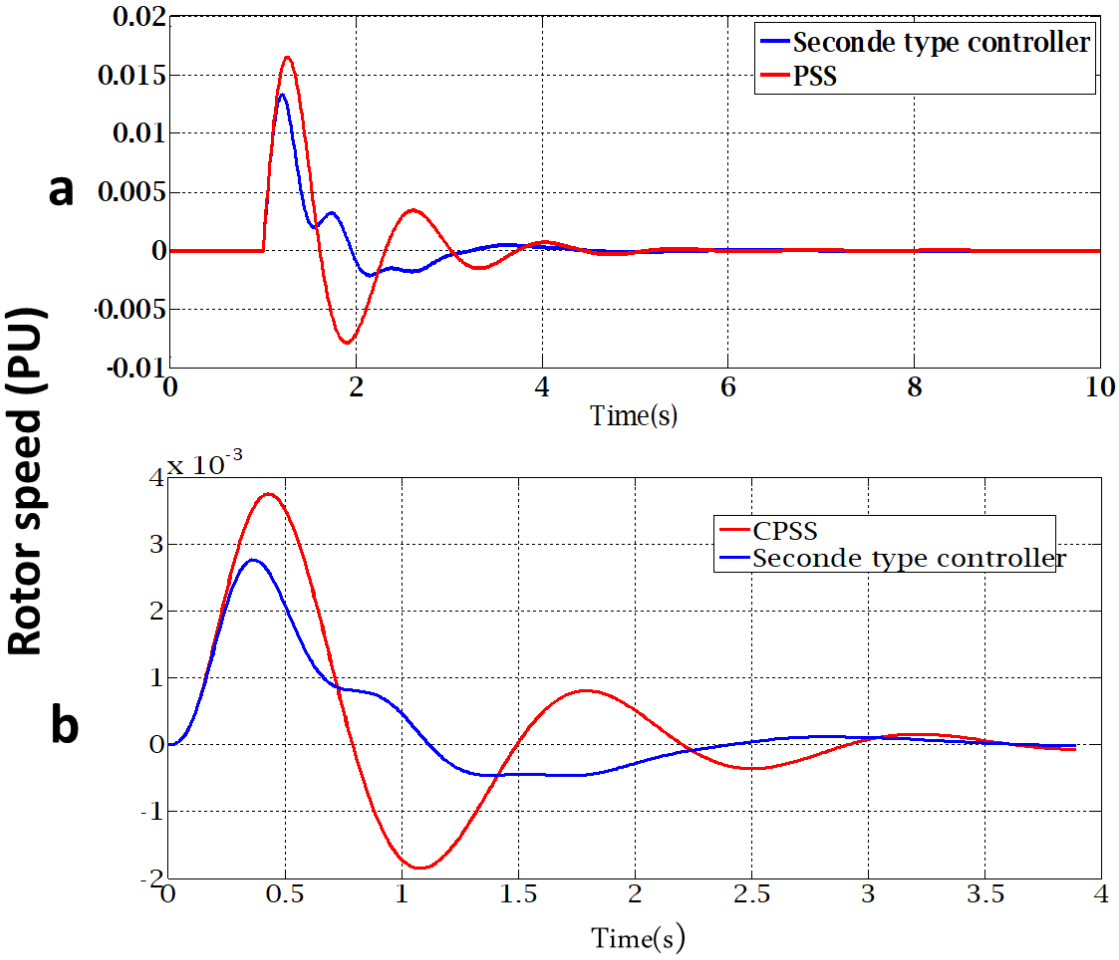
a
b
Rotor speed (PU)
Seconde type controller
PSS
Time(s)
x 10^-3
CPSS
Seconde type controller
Time(s)

Fig. 13

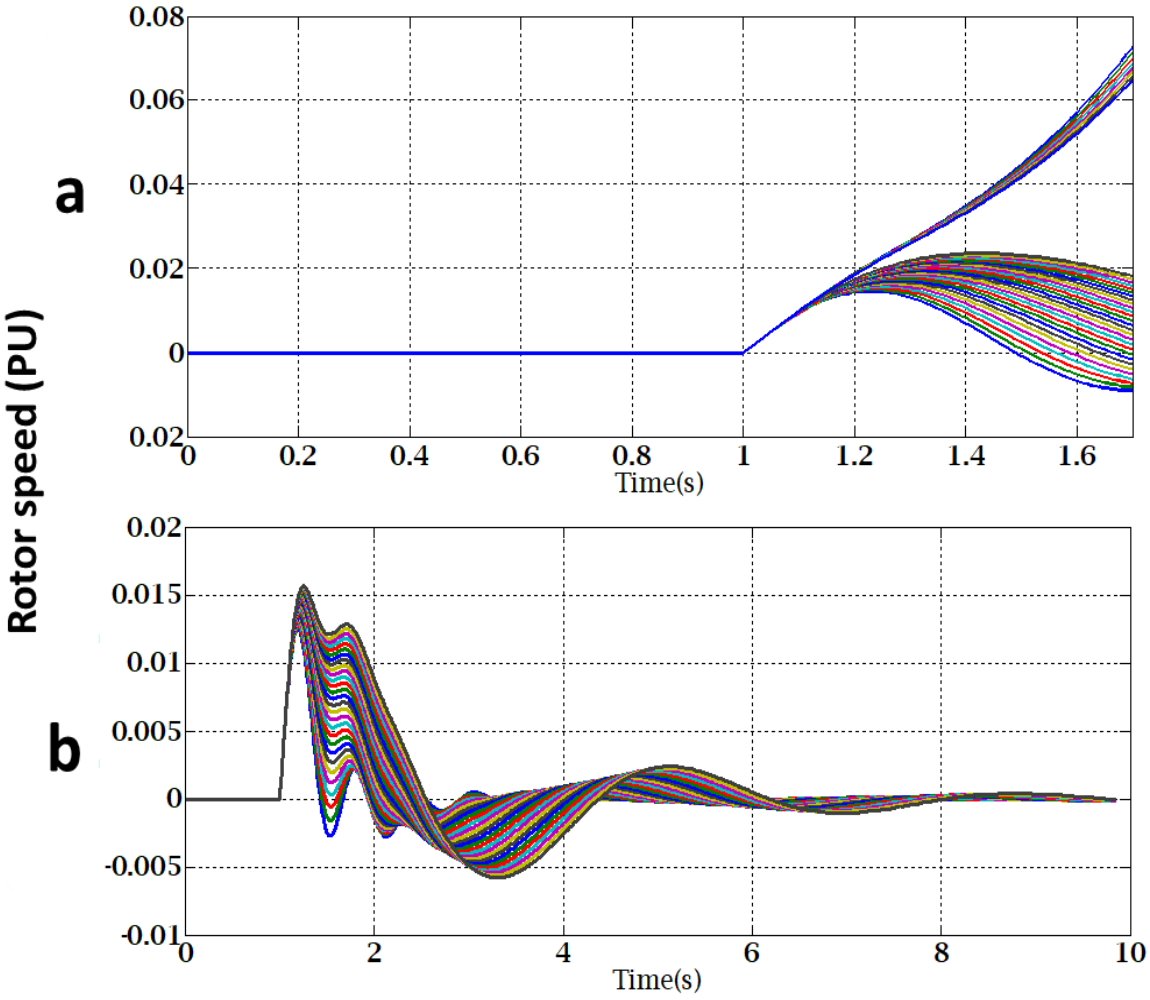
a
b
Rotor speed (PU)
Time(s)
Time(s)
0.08
0.06
0.04
0.02
0
0.02
0.2
0.4
0.6
0.8
1
1.2
1.4
1.6
0.02
0.015
0.01
0.005
0
-0.005
-0.01
2
4
6
8
10

Fig. 14

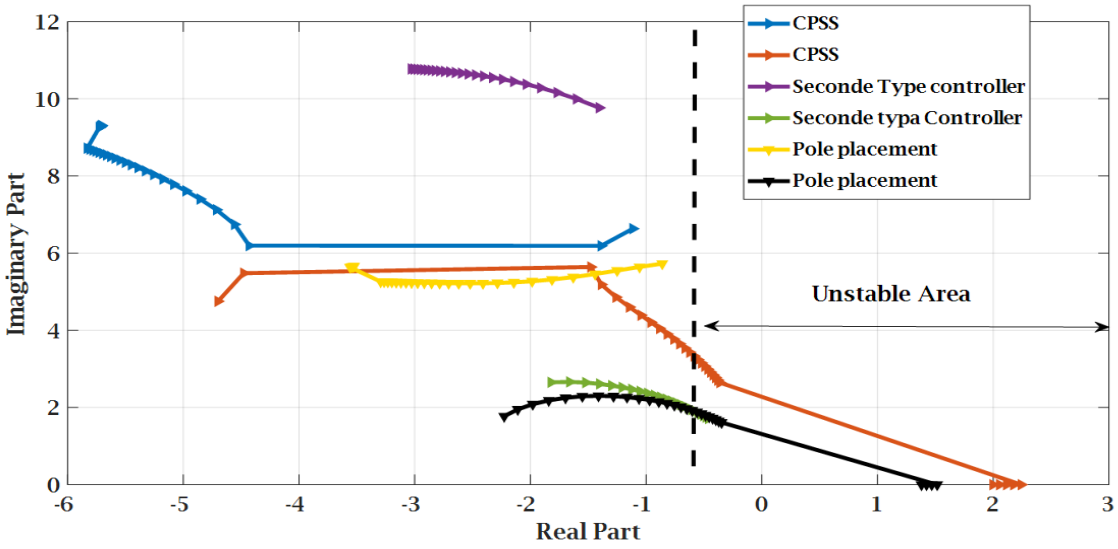
CPSS
CPSS
Seconde Type controller
Seconde typa Controller
Pole placement
Pole placement
Unstable Area
Imaginary Part
Real Part
12
10
8
6
4
2
0
-6
-5
-4
-3
-2
-1
0
1
2
3

Fig. 15

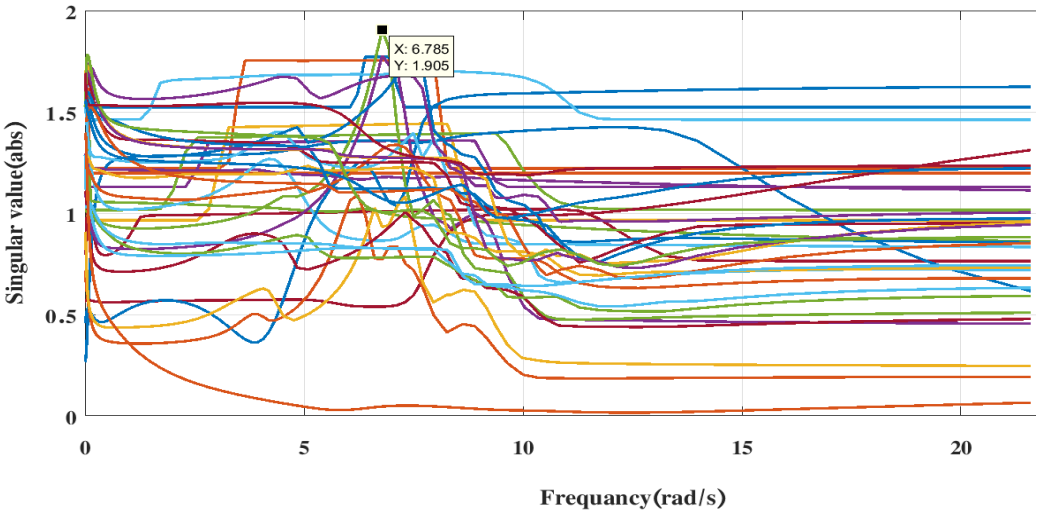
X: 6.785
Y: 1.905
Singular value(abs)
Frequancy(rad/s)
0
0.5
1
1.5
2
0
5
10
15
20

Fig. 16

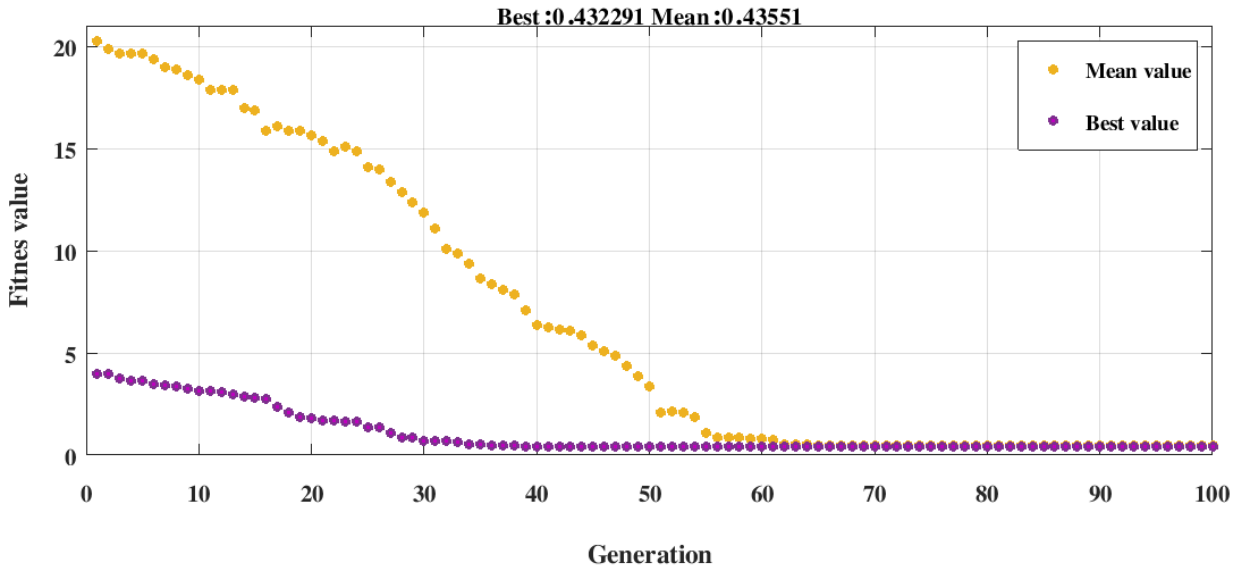
Best :0.432291 Mean :0.43551
Mean value
Best value
Fitnes value
Generation
0
5
10
15
20
0
10
20
30
40
50
60
70
80
90
100

Fig. 17

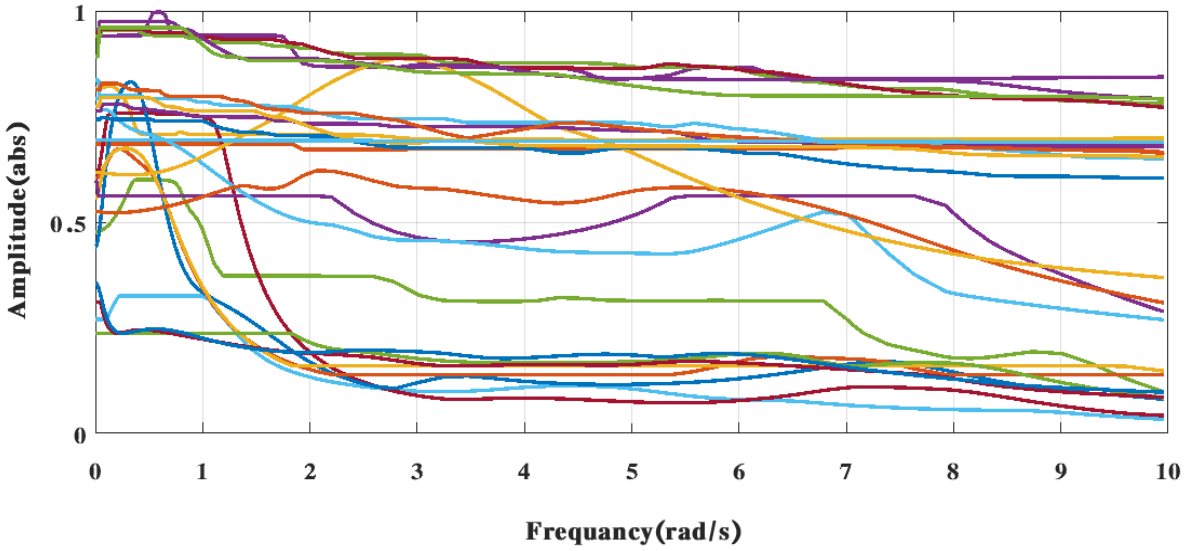

Fig. 18

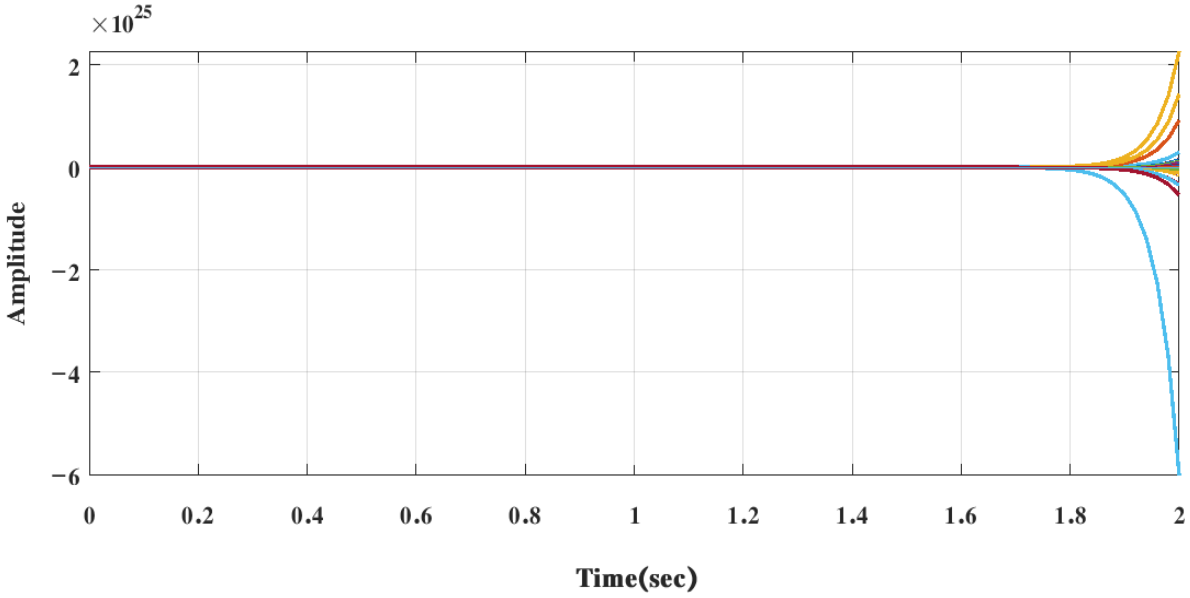

Fig. 19

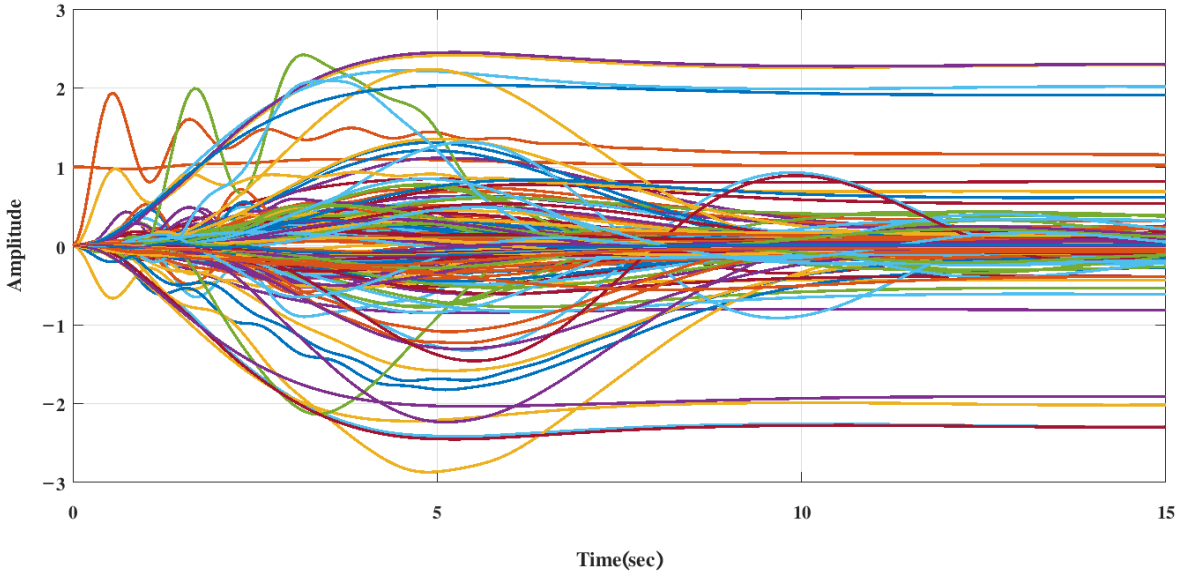

Fig. 20

Mode Type (Stable/Unstable)	Eigenvalues
Stable	-23.4550
Stable	-0.0909
Stable	-22.84
Stable	-11.203+4.905j -11.203-4.905j
Unstable	1.06913+6.3672j 1.06913+6.3672j

Table I

Variable	Value
T_{r1}	0.13406
T_{r2}	0.5486
T_1	0.1
T_2	-0.2417
T_w	5
K_{Cp}	9.454
K_{RC}	58.486
T_{Cp}	9.454

Table II

Mode Type (Stable/Unstable)	Eigenvalues
Stable	-16.6649
Stable	-10.56417
Stable	-7
Stable	-0.2417
Stable	-9
Stable	-150187+2.8098j -150187-2.8098j
Stable	-2.04119+8.5239j -2.04119-8.5239j

Table III

PSS_name	GEN2	GEN3	GEN4	GEN5	GEN6	GEN7	GEN8	GEN9	GEN10
K_{cp}	0.4999	0.500	2	1	4.000	7.490	2	2	**1**
T_1	9.5100	12.26	2.4580	4.4263	1.5252	0.8390	3.0536	3.3880	**5.4061**
T_2	0.0708	0.709	0.0688	0.0528	0.0276	0.0160	0.0552	0.0812	**0.0437**
T_3	5	5	5	5	5	5	5	5	**5**

Table IV

Mode Number	Real part	Imaginary part	Frequency	Damping ratio	Mode Type(Stable/Unstable)
1	-0.2849172	6.9986454	1.1138690	0.0406766	Stable
2	-0.3850304	6.6149199	1.0527972	0.0581080	Stable
3	-0.4641656	7.5177541	1.1964877	0.0616252	Stable
4	-0.4195530	6.1520555	0.9791300	0.0680391	Stable
5	-0.5764449	7.4772932	1.1900481	0.0768646	Stable
6	-0.6957257	8.9392823	1.4227309	0.0775932	Stable
7	-0.3140888	4.0118904	0.6385121	0.0780506	Stable
8	-0.7388887	8.8669296	1.4112156	0.0830430	Stable
9	-0.8204883	9.1112823	1.45010562	0.089688	Stable

Table V

R_cNo	**GEN2**	**GEN3**	**GEN4**	**GEN5**	**GEN6**	**GEN7**	**GEN8**	**GEN9**	**GEN10**
K_{cp}	4.9949	1.021	3.25	1.355	1.376	3.3167	4.0650	1.2815	3.8869
T_{r1}	4.987	1.095	1.9397	3.558	4.622	0.7268	1.5708	0.3380	0.1456
T_{r2}	1.1935	4.527	0.725	0.739	0.0115	3.4932	4.8084	4.8752	2.9624

Table VI

Biography:

Sadegh Kamali received the MSc and Ph.D. degrees in power system engineering from K.N. Toosi University of Technology, Tehran, Iran in 2014 and 2019, respectively. His research interests are power system dynamics, and power system control.

Masoud Hasani Marzooni received the B.Sc., M.Sc., and Ph.D. degrees in electrical engineering from Sharif University of Technology, Tehran, Iran, in 2001, 2004, and 2011, respectively. He is currently an assistant professor with the energy and electricity economics department at Niroo Research Institute, Tehran, Iran. His current research interests include power system dynamics, power system planning and operation, smart grid and power system economics.

Turaj Amraee received the Ph.D. degree in power system engineering from the Sharif University of Technology, Tehran, Iran, in collaboration with Grenoble-INP University, Grenoble, France, in 2010. He is currently an associate professor with the electrical engineering department at K.N. Toosi University of Technology, Tehran, Iran. His research interests are smart grid, power system planning, power system dynamics, renewable energies, and microgrids.